Comparison of Porous Germanium Thin Films on SS and Mo as Anode for High-Performance LIBs

Valentina Diolaiti, Alfredo Andreoli, Susana Chauque, Paolo Bernardoni, Giulio Mangherini, Marco Ricci, Remo P. Zaccaria, Matteo Ferroni, and Donato Vincenzi

***Abstract*—The increasing demand for high performance lithium ion batteries is pushing the research toward the development of new materials for electrodes. Our study focuses on the usage of Germanium as the active material for the negative electrode since it has a higher theoretical specific capacity than standard graphite-based electrodes. This research article provides insight into the electrochemical performance of thin films of Germanium deposited on metallic substrates and then nanostructured via electrochemical etching. Molybdenum and stainless steel are investigated as substrates and compared with regard to the performance of the resulting electrodes. The nanostructured Germanium electrodes show promising results, demonstrating a stable and high specific capacity for hundreds of cycles. The long-term stability of the cell together with a high rate capability proves the reliability of the cell engineered.**

***Index Terms*—Nanostructured Germanium, PECVD, electrochemical etching, high capacity anode material, LIBs.**

I. Introduction

NOWADAYS, lithium-ion batteries (LIBs) are a well-known industrial technology, widely used in high-tech fields and in the renewable energy sector. The forthcoming green transition has boosted the storage of electrical energy for wind and solar power [1], [2] in order to decrease the direct carbonaceous emissions. LIBs have an efficient storage mechanism hence could be used as storing devices for stationary applications [3] but a long lifetime needs to be guaranteed. The most common LIBs exploit insertion-type materials that, due to their intrinsic nature, have a limited storage capacity and therefore a low energy density. As an alternative, alloying materials, i.e. Silicon, Germanium, and Tin, are under strong scientific investigation for their high theoretical specific capacity. Among them, Germanium (Ge) has been deemed promising as anodic material for LIBs. Indeed, it shows superior electronic properties with respect to Silicon demonstrating a higher intrinsic electronic conductivity due to the smaller band gap [4] and a better lithium-ion diffusivity [5] thus proving its suitability to be employed as LIB negative electrode.

The Ge higher conductivity is directly related to its high carrier mobility of 1800 $cm^2\ V^{-1}\ s^{-1}$ and 3600 $cm^2\ V^{-1}\ s^{-1}$ for holes and electrons respectively [6], which results in an intrinsic conductivity at room temperature three orders of magnitude higher than Si [7], [8], [9].

The redox reactions of Ge with metallic lithium result in a high theoretical specific capacity of 1624 mA h g^{-1} (vs. the 372 mA h g^{-1} of standard graphite electrodes). The reaction mechanism evolves through the formation of lithium-germanium alloys with different stochiometry leading to the formation of $Li_{15}\ Ge_4$ as a discharge product.

Notably, Ge-based anodes demonstrate high rate capability performance thanks to their good conduction properties [10]. However, Ge undergoes a drastic volume expansion upon lithiation and de-lithiation which causes the electrode pulverization leading to active material losses and poor electrical contact. Moreover, the material pulverization determines a continuous exposure of new Ge surface that reacts with the electrolyte to form the solid electrolyte interphase (SEI) thus reducing the lithium inventory within the cell. Both these effects contribute to the overall reduction of the battery deliverable capacity.

Many strategies have been proposed or are currently studied to render these materials available as long-term solutions for LIB anodes. One way is to mix or co-structure them with carbon-based composites, which could act as a buffer for the volumetric expansion [11]. Of course, this reduces the overall gravimetric capacity, but still results in a much higher capacity than graphite, while helping to alleviate the cycle-life challenges [12]. Another promising solution is represented by the nano-structuration of the active materials. This has the potential to reduce the stress and

Manuscript received 7 July 2023; accepted 26 August 2023. Date of publication 7 September 2023; date of current version 14 September 2023. This work was supported by the Italian Space Agency, in the framework of the invitation to tender New Ideas for Future Space Tools (ASI loan Agreement Number 2018-1-U.O) through Project ANGELS (ANodi in GErmanionanoporoso per batterie al Litio per applicazioni aeroSpaziali), and in the framework of the invitation to tender Interdisciplinary Enabling Technologies (ASI loan Agreement Number 2021-2-U.0) through Project GLITTERY(GermaniumLithium-Ion baTTERY). This work was supported by the Italian Space Agency (ASI). The review of this article was arranged by Associate Editor X. Sun. *(Corresponding authors: Valentina Diolaiti; Alfredo Andreoli.)*

Valentina Diolaiti is with the Physics, University of Ferrara, 44121 Ferrara, Italy (e-mail: valentina.diolaiti@unife.it).

Alfredo Andreoli, Giulio Mangherini, and Donato Vincenzi are with the Physics and Earth Science, University of Ferrara, 44121 Ferrara, Italy (e-mail: alfredo.andreoli@unife.it; giulio.mangherini@unife.it; donato.vincenzi@unife.it).

Susana Chauque and Marco Ricci are with the Istituto Italiano di Tecnologia, 16163 Genova, Italy (e-mail: susana.chauque@iit.it; marco.ricci@iit.it).

Paolo Bernardoni is with the Department of Chemical, Pharmaceutical and Agricultural Sciences, University of Ferrara, 44121 Ferrara, Italy (e-mail: paolo.bernardoni@unife.it).

Remo P. Zaccaria is with the Italian Institute of Technology, 16163 Genova, Italy (e-mail: remo.proietti@iit.it).

Matteo Ferroni is with the DICATAM, University of Brescia, 25121 Brescia, Italy (e-mail: matteo.ferroni@unibs.it).

This article has supplementary downloadable material available at https://doi.org/10.1109/TNANO.2023.3311757, provided by the authors.

Digital Object Identifier 10.1109/TNANO.2023.3311757

strain associated with the expansion [12] so that the material can reversibly accommodate it. Furthermore, besides relieving the volume variation, nano-structuration offers several additional advantages, like an enhanced surface-to-volume ratio leading to more active sites available for lithium storage, and a larger surface in contact with the electrolyte resulting in a better ionic transfer and reduced diffusion lengths [13]. Recent studies show how 3D printed nanostructures can be used to produce electrodes in a cost effective way [14].

Herein, a comparison of the electrochemical nanostructuring process of Ge electrodes deposited by plasma-enhanced chemical vapor deposition (PECVD) on two different substrates, molybdenum (Mo) and stainless steel (SS) is reported. The physical and electrochemical study on Mo was previously reported by our group [15], [16] as Ge substrate due to its good electrical properties and high melting point, while SS is here explored as an alternative material owing to its compatibility with the fabrication process and its wider availability. The proposed deposition process enabled us to boast the rate capability and guarantees a stable capacity for more than 200 cycles.

II. Binder-Free Anode Fabrication

The binder-free anodes proposed in this article are fabricated by depositing Ge via PECVD on top of a metallic substrate thus ensuring electrical conductivity. PECVD is a chemical vapor deposition technique assisted by a plasma ignited with a radio frequency of 13.56 MHz. GeH_4 is employed as gas precursor for the Ge deposition. The samples are hosted in a quartz holder placed above an inlet gas ring. A graphite heater located above the sample holder enables the constant control of the temperature during the process. The deposition rate was calculated from a profile measurement and secondary-ion mass spectrometry (SIMS) analysis and its value is estimated to be 1.26 nm s^{-1}. The substrate of choice is a high-melting-point metal with low vapor pressure in order to avoid contaminating the deposition chamber. Furthermore, the substrate needs to be resistant to hydrofluoric acid (HF) since the porous structures are created via electrochemical etching in HF. For this purpose, Mo and SS are selected and compared as Ge supporting materials. Before the deposition, all the substrates are rinsed in dichloromethane, acetone, isopropanol and de-ionised water in order to remove organic impurities. The deposition occurs at a pressure of about 10^{-3} mbar inside the deposition chamber in which the substrate is heated up above 400 °C. The plasma deposition time was set to 14 minutes.

III. Nanostructuring

Due to the typical volumetric expansion of alloy-type anodes upon repeated charge and discharge, the Ge film needs to be nanostructured for its efficient application as an electrode in LIBs [17]. This process is realized via electrochemical etching in a solution composed by aqueous HF (50% diluted, MOS grade, CARLO ERBA reagents) and ethanol (RS grade, CARLO ERBA Reagent) in a ratio of 3:1 v:v. The experimental set-up is made of a polytetrafluoroethylene (PTFE) tank and an aluminum (Al) plate acting both as a support and current collector, as shown in Fig. 1. A graphite rod is connected to the negative terminal of a

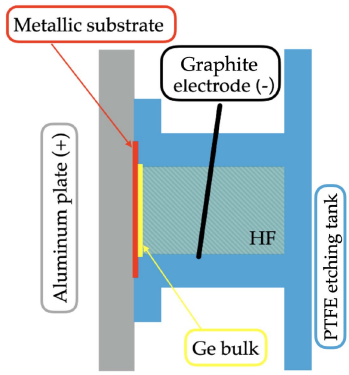

Fig. 1. Set up for the electrochemical etching representing, the PTFE etching tank, the graphite rod, the Al plate, the metallic substrate and the Ge bulk deposited on the metallic substrate.

Keithley 2400, while the positive terminal is connected to the Al plate. The anodic dissolution is achieved using a 40 mA current for 180 s controlled by a LabView VI customly developed for this process.

As known from the literature, there are mainly two reactions taking place during germanium electrochemical etching: the divalent and the tetravalent reactions. The divalent reaction is

$$Ge + 6HF + 2\,h^+ \rightarrow GeF_6^{2-} + 4H^+ + H_2 \qquad (1)$$

while the tetravalent one is expressed as

$$Ge + 6HF + 4\,h^+ \rightarrow GeF_6^{2-} + 6H^+ \qquad (2)$$

The theoretical models proposed by Dupuy et al. attribute the tetravalent reaction to the vertical growth of the pores, whilst the divalent process is foreseen to be responsible for the constant dissolution of the already-porous region, gradually increasing the pore diameter, and reducing the layer thickness [18].

Specific surface areas of the SS samples were determined by applying the Brunauer-Emmett-Teller (BET) method to the absorption/desorption isotherms obtained with a Micromeritics ASAP 2020 physisorption analyzer. The adsorption/desorption isotherms were determined over a wide range of relative pressures ($10^{-6} < p/p_0 < 1$). All samples underwent an activation step to remove physisorbed species from the surface while avoiding irreversible changes of the solid structure. Each sample was studied after outgassing in vacuum at 120 °C (heating ramp of 5 °C/min) for 2 hours (residual pressure of 10^{-4} mbar). The superficial area obtained with Kr is equal to 0.0098 $m^2\,g^{-1}$, almost twice the electrode geometric area. This measurement is affected by a 5% experimental error due to the possible deformation of the probe molecule and only a superficial area measurement is possible. Porosity measurements were not possible using Kr.

IV. Micro-Structural Characterisation

The morphology and microcrystalline arrangement of the Ge films have been investigated by scanning electron microscopy (SEM) and transmission electron microscopy (TEM). A thin cross-section of the Ge layers deposited on Mo or SS has been prepared by focused ion beam (FIB-SEM) to complement the standard top-view SEM observation of the porosity of the

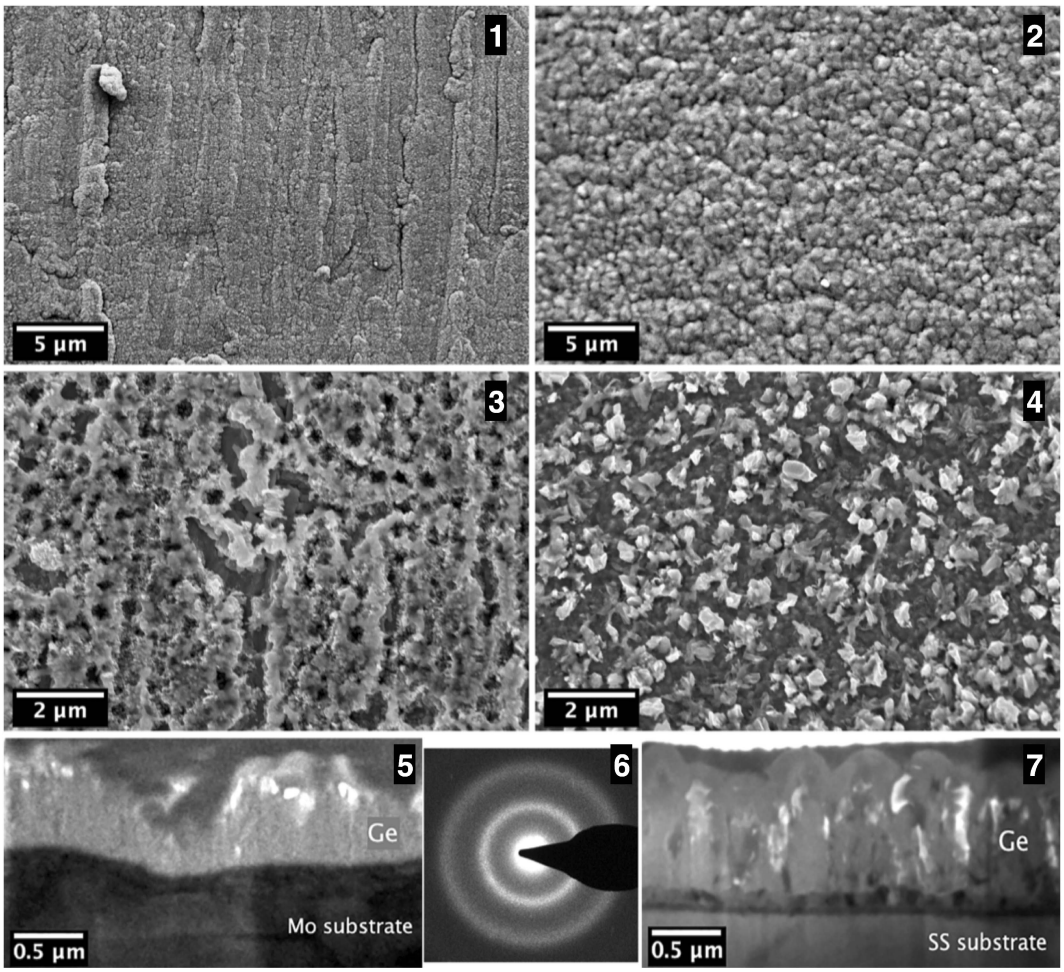

Fig. 2. Comparison between the Ge layers deposited over Mo and SS substrates. TOP:SEM images of the bulk Ge layers after PECVD deposition on Mo (1) [15] and SS (2) substrates. The deposited Ge layers are homogeneous and feature a nanosized morphology. CENTER: SEM images of the porous Ge layers on Mo (3) [15] and SS (4). The electrochemical process promoted formation of an open porosity at the layer surface. The modification of the layer is uniform. BOTTOM: Cross sectional TEM bright-field view of the porous Ge layers on Mo (5) and SS (7) substrates, showing that the porosity in the Ge nanostructured film extends through the layers thickness. The electron diffraction pattern (6) indicates a nanostructured metallic Ge phase for both porous layers.

Ge films. The comparative investigation of the microstructural features of the Ge layers deposited on either Mo or SS is functional to the optimization of the fabrication process and to the description of the electrochemical performance of the material. In addition to conventional TEM imaging and electron diffraction, the scanning-transmission high-angle annular dark-field mode (STEM-HAADF) was exploited in association with energy dispersive X-ray spectroscopy to enhance the compositional contrast and measure the elemental distribution. The morphology of the Ge layers right after deposition on Mo and SS substrates is shown in Fig. 2 (1–2). The Ge layers appear to be compact and uniform over the entire deposition area. For the sample deposited on the laminated Mo substrate, a large striation conformal to the underlying substrate is evident. On the other hand, the Ge deposited on SS shows a granular morphology uniformly distributed over the substrate. In addition, a dense nanometric morphology has been promoted by the deposition of the Ge layers from the PECVD process. Fig. 2 (3–4) shows the Ge morphology at higher magnification, highlighting the effect of electrochemical treatment on the Ge layers, with a large open porosity visible on both the samples as reported in [15]. The obtained porosity is believed to play an essential role in the volumetric expansion during lithiation and de-lithiation processes. The vertical striation in the sample deposited on Mo appears to assist the etching and the porosity attains the substrate. Nevertheless, the Ge layer remains attached to the substrates and no evidence of delamination has been observed. The etching process on the sample deposited on SS creates a network of prominent nanometric structures over a relatively compact and dense layer. Also in this case an adequate adhesion of the Ge film on the substrate was preserved.

TEM analysis, reported in Fig. 2 (5–7), address the extent of porosity and the micro-structures of both Ge layers. For the sample deposited on Mo, the layer thickness measured from the cross-sectional samples is in the range between 0.25 and 0.64 μm. These values are compatible with the initial thickness and the consequent reduction due to the electrochemical process.

For the sample deposited on SS, the thickness features higher uniformity and measures about 1.3 μm. The Ge layer shows a

large porosity and, differently, a dense and compact morphology is visible from about 90 nm to the interface with the substrate. An incomplete pore formation, likely caused by an initial layer thickness higher than estimated, could provide an explanation for the evidence.

The absence of contrast from crystalline domains in the TEM images suggests a low degree of crystallinity for both the Ge layers. The electron diffraction pattern, Fig. 2 (6), supports this finding as it is characterized by uniform and diffuse concentric intensity rings. Such a pattern indicates a nanometric size and absence of preferential orientation for the crystalline domains. The lattice spacing measured from the electron diffraction pattern agrees with the metallic-Ge phase also recorded from X-Ray Diffraction measurements, as it can be ascertained from Fig. S1 and related description in the supplementary information.

V. Electrochemical Analysis

For the electrochemical characterization, the porous Ge-based electrodes (PGe) were tested in CR 2032 coin-type cells assembled in a half-cell configuration using metallic lithium (0.6 mm thick) as counter and reference electrode. The final PGe anodes are punch cut into 15 mm diameter disks and have a thickness of 0.026 mm. The electrode mass loading for the PGe on Mo is 0.25 mg while for the PGe on SS is 0.26 mg. The electrodes are separated by a glass fiber membrane (Whatman GF/D) soaked with 200 μL of an electrolytic solution composed by 1 M $LiPF_6$ in a 1:1 v:v mixture of ethylene carbonate (EC) and dimethyl carbonate (DMC). To enhance and stabilize the electrochemical performances of the electrodes, 10 wt.% FEC is used as additive for the electrolytic solution [19], [20]. The coin cells were assembled using a digital pressure controlled electric crimper MSK-160E. The cyclic voltammetry (CV), galvanostatic charge/discharge cycles and rate capability tests were performed at room temperature using a BioLogic BCS-805 multichannel battery unit controlled by BT Lab software.

The CV curves performed within $[0.01 - 1.5]$ V at a scan rate of 0.1 mV s^{-1} for both PGe-based anodes (PGe on Mo and SS) are shown in Fig. 3. Some of the reduction peaks of the 1st cycles correspond to the SEI formation on the electrode surface. The organic solvents composing the electrolyte partially react during the first discharge, generating the SEI, which acts as a protective layer against side reactions and enabling only lithium ions to cross it [21]. The SEI formation is also responsible for the initial irreversible capacity loss of the cell since Li^+ ions that are provided by the cathode during the first cycle are trapped inside this layer [22]. In order to prevent further side reactions, the SEI needs to be stable and dense. For Ge, as for Si, the significant volume change makes it difficult to establish a compact SEI, and may even cause its fracturing. This results in an additional exposure of Ge surface to the electrolyte which leads to the thickening of this protective layer upon cycling.

The CV peaks are identified from comparisons with the literature. Specifically, in the Mo 1st cycle, a clear reduction peak at around 0.54 V is observed followed by other two at 0.27 V and 0.13 V. The first peak in the cathodic scan is attributed to the SEI formation [23]. At potentials up to around 0.25 V, c-Ge is converted in Li_7Ge_3 phase. At lower potential a structural

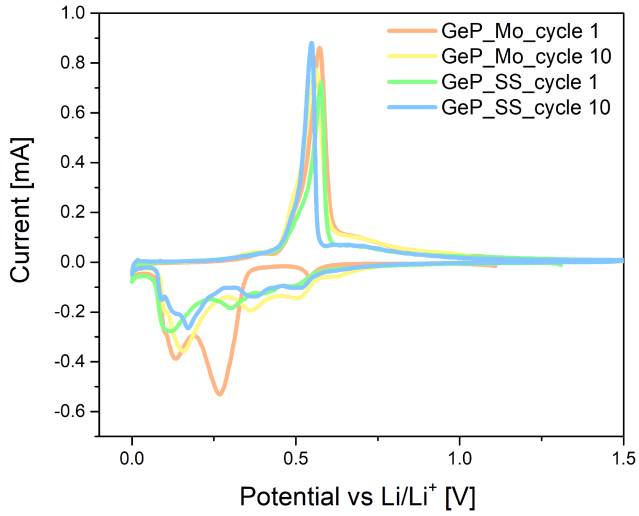

Fig. 3. Cyclic voltammetry curves of PGe on Mo and SS substrate materials at a scan rate of 0.1 mV s^{-1} within [0.01–1.5] V. The first cycles are reported together with the 10th cycles. Cycles 1 and 10 of Mo are taken from [15].

transformation of the Li_7Ge_3 to the Li_7Ge_2 amorphous phase occurs. For potentials between 0.15 V and 0 V, the conversion from Li_7Ge_2 to the $Li_{15}Ge_4$ phase takes place [10]. In the anodic scan, the broad peak at 0.6 V is related to the delithiation process of all the Li-Ge phases formed previously, and results in a-Ge [24], [25].

The reduction curves of the 10th cycles and of the 1st cycle of the SS sample share a similar behavior, which is anyway different from that of the 1st cycle of the Mo sample. In particular, a multiple peak structure shifted towards higher potential is observed. The main cathodic peaks are found at about 0.5 V, 0.35 V, and 0.17 V, and could be ascribed to the multistep lithiation of a-Ge [4], [16], [25]. Interestingly, a high similarity can be recognised with the differential capacity plot (DCP) curves shown in Fig. S2, with peaks at similar potential values. An hypothesis for the difference between the 1st cycles could be a different content of c-Ge phase in the pristine samples, with the SS one showing a lower amount of crystalline material. The small cathodic peak of the SS sample around 0.3 V, which disappears in the following cycles, could be ascribed to lithiation of c-Ge supporting this hypothesis.

The slight difference in the current intensity, found for both materials during the first 10 cycles, could be related to the stabilization of the half-cells. It is important to note that all the CV curves have similar shape since the active material is PGe both on Mo and SS and the almost identical redox peak positions for both substrates indicate that the same conversion reactions take place on the surface. The slight difference in the cathodic region could be due to the presence of different Li-Ge amorphous phases whose deep investigation falls out the scope of the present work and will be the subject of a following study.

Fig. 4 shows the rate capability performance of both PGe deposited on Mo (a) and SS (b) over cycling at various C-rates (C/10, C/8, C/4, C/2, 1 C, 2 C, 4 C, 8 C, 10 C, 20 C, 40 C, 60 C and finally back at C/10). The first cycles are taken at very low currents to allow the SEI formation and the stabilization of the active material [26]. For instance, the specific discharge capacity

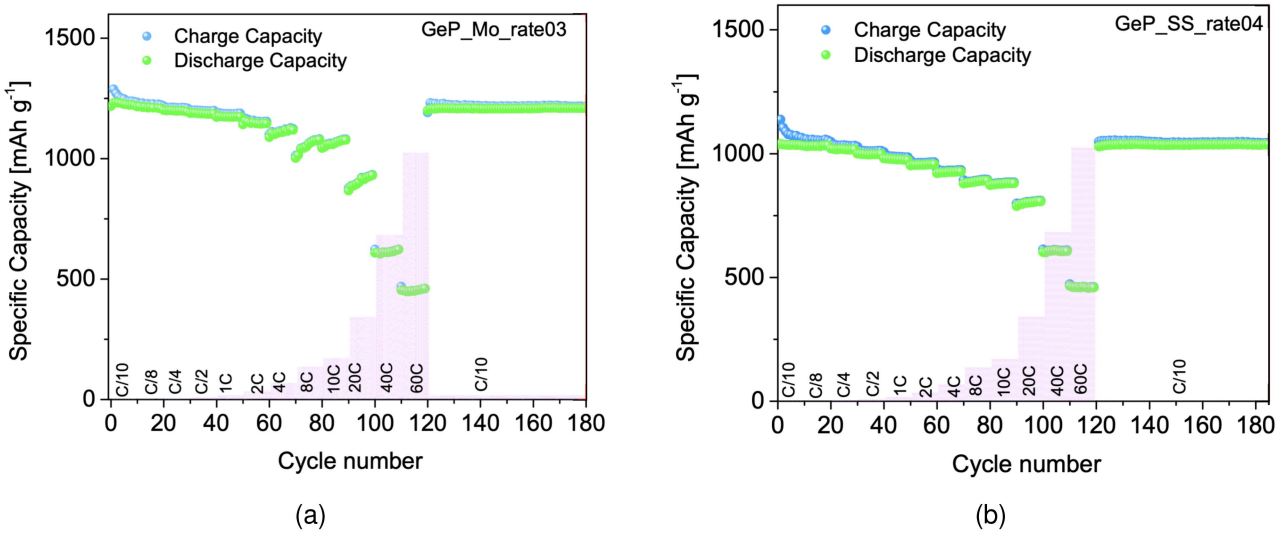

Fig. 4. Rate capability of the PGe on Mo (a) (adapted with copyright permission from [16]) and SS (b) anodes over cycling at different current densities within [0.01–1.5]V.

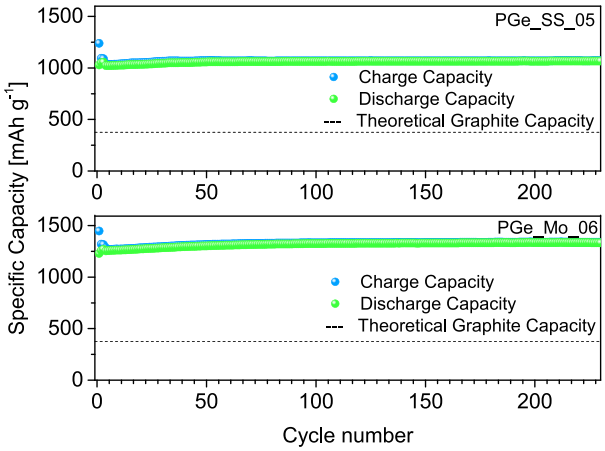

Fig. 5. Cycling performance of Ge anode on both PGe on Mo (adapted from [15]) and PGe on SS at a current rate of 1 C within [0.01–1.5] V.

for PGe deposited on Mo is around 1130 mA h g^{-1} and 875 mA h g^{-1} at 4 C and 20 C, respectively. On the other hand, for the PGe deposited on SS these values are around 910 mA h g^{-1} and 800 mA h g^{-1} at 4 C and 20 C, respectively. For both PGe-based anodes a remarkable response is obtained in the specific capacity at very high rates (40 C and 60 C), which for the SS sample is slightly below 500 mA h g^{-1}. Furthermore, once the cells were cycled back at C/10, the initial specific capacity was recovered in both cases (i.e. 1250 mA h g^{-1} for PGe on Mo and 1000 mA h g^{-1} for PGe on SS), meaning that the here proposed PGe-based anodes have no memory effect.

The cycling performance of the PGe-based electrodes at 1 C (corresponding to 1624 mA g^{-1}) are shown in Fig. 5. The same specific capacity values obtained in the rate capability tests are reproduced, being around 1250 mA h g^{-1} for the cell with Mo substrate and 1000 mA h g^{-1} for the PGe onto SS. It is important to remark the obtained great stability in the specific capacity values over more than 200 cycles.

Additionally, a better response both in rate capability and long-cycling tests is obtained in the case of PGe on Mo rather than PGe on SS. The difference in the specific capacity could be related to the higher electrical conductivity of Mo than SS and to a thicker interface forming on SS reducing the effective mass loading of the anode. The latter could take up active PGe material which will not be available for the lithium alloying reactions. Nevertheless the application of the SS as a suitable substrate of Ge as active material for anodes of LIBs has been vastly demonstrated.

As mentioned above, in Fig. S2 the differential capacity of the galvanostatic charge/discharge curves have been plotted corresponding to the 185th cycle for both PGe-anodes after the rate capability and long cycling tests. Analogously to the CV tests, it is possible to observe the same shapes for both PGe on Mo and PGe on SS electrodes. They also present a great stability even after being tested at high current regimes, as in the case of the rate capability experiments.

VI. Conclusion and Outlook

With this work, we demonstrated the potential of nanostructured PGe electrodes for lithium-ion batteries. These electrodes revealed a specific capacity over three times higher than standard graphite and an impressive stability over cycling. The nanostructured PGe electrodes described here were also able to retain their performance at a relatively high current. Moreover, they were able to recover their original capacity after current spikes up to 60 C. The excellent reliability and rate capability of these electrodes can be ascribed to the nanostructure obtained with the proposed fabrication process. The porous layer can accomodate the expansion and contraction during lithiation and de-lithiation. Additionally, the nanostructure allows an optimal electrode-electrolyte contact, minimizing the rate limitations of the electrodes.

Thanks to its high and stable capacity, this type of electrodes could also be used in solid-state battery applications where the parasitic reactions are suppressed, theoretically improving even more the GeP electrode performances [27].

In conclusion, this work is a step in the research to achieve the practical viability of Ge in lithium-ion cells, proving that a cheap and industrially-oriented material like SS can be used in place of Mo as a substrate with only minimal performance costs. The reason between the slight performance difference between Ge electrodes supported on Mo and SS is currently under investigation.

ACKNOWLEDGMENT

Part of the descriptions of the present work are taken or adapted from the previous contributed paper [15], in agreement with TNANO ethical policy.

A sincere thanks to Eleonora Venezia for her academic support and to Silvio Fugattini for his notable help during the project.

REFERENCES

[1] W. A. Braff, J. M. Mueller, and J. E. Trancik, "Value of storage technologies for wind and solar energy," *Nature Climate Change*, vol. 6, no. 10, pp. 964–969, 2016.

[2] G. Mangherini, P. Bernardoni, E. Baccega, A. Andreoli, V. Diolaiti, and D. Vincenzi, "Design of a ventilated façade integrating a luminescent solar concentrator photovoltaic panel," *Sustainability*, vol. 15, no. 12, 2023, Art. no. 9146.

[3] J. B. Goodenough and K.-S. Park, "The Li-ion rechargeable battery: A perspective," *J. Amer. Chem. Soc.*, vol. 135, no. 4, pp. 1167–1176, 2013.

[4] G. Chen et al., "Revealing capacity degradation of ge anode triggered by interfacial LiH evolution," *Angewandte Chemie*, vol. 135, 2023, Art. no. e202306141.

[5] I. Gavrilin et al., "Study of the process of reversible insertion of lithium into nanostructured materials based on germanium," *Russian J. Electrochemistry*, vol. 54, pp. 1111–1116, 2018.

[6] C. Kittel and P. McEuen, *Introduction to Solid State Physics*. Hoboken, NJ, USA: Wiley, 2018.

[7] A. Levitas, "Electrical properties of germanium-silicon alloys," *Phys. Rev.*, vol. 99, no. 6, 1955, Art. no. 1810.

[8] G. Eranna, *Crystal Growth and Evaluation of Silicon for VLSI and ULSI*. Boca Raton, FL, USA: CRC Press, 2015.

[9] D. W. Thomas, T. Mahmood, and C. B. Lindahl, *Germanium and Germanium Compounds*. Hoboken, NJ, USA: Wiley, 2004. [Online]. Available: https://onlinelibrary.wiley.com/doi/abs/10.1002/0471238961.0705181301040113.a01.pub3

[10] X. Liu, X.-Y. Wu, B. Chang, and K.-X. Wang, "Recent progress on germanium-based anodes for lithium ion batteries: Efficient lithiation strategies and mechanisms," *Energy Storage Mater.*, vol. 30, pp. 146–169, 2020.

[11] D. Li, H. Wang, H. K. Liu, and Z. Guo, "A new strategy for achieving a high performance anode for lithium ion batteries–encapsulating germanium nanoparticles in carbon nanoboxes," *Adv. Energy Mater.*, vol. 6, no. 5, 2016, Art. no. 1501666.

[12] J. T. Warner, *Lithium-Ion Battery Chemistries: A Primer*. New York, NY, USA: Elsevier, 2019.

[13] X. Zhang, X. Cheng, and Q. Zhang, "Nanostructured energy materials for electrochemical energy conversion and storage: A review," *J. Energy Chem.*, vol. 25, no. 6, pp. 967–984, 2016.

[14] X. Gao, M. Zheng, X. Yang, R. Sun, J. Zhang, and X. Sun, "Emerging application of 3D-printing techniques in lithium batteries: From liquid to solid," *Mater. Today*, vol. 59, pp. 161–181, 2022.

[15] V. Diolaiti et al., "Nanostructured germanium anode for lithium-ion batteries for aerospace technologies," in *Proc. IEEE 22nd Int. Conf. Nanotechnol.*, 2022, pp. 56–59.

[16] S. Fugattini et al., "Binder-free nanostructured germanium anode for high resilience lithium-ion battery," *Electrochimica Acta*, vol. 411, 2022, Art. no. 139832.

[17] P. Moriarty, "Nanostructured materials," *Rep. Prog. Phys.*, vol. 64, no. 3, 2001, Art. no. 297.

[18] A. Dupuy, M. R. Aziziyan, D. Machon, R. Arés, and A. Boucherif, "Anisotropic mesoporous germanium nanostructures by fast bipolar electrochemical etching," *Electrochimica Acta*, vol. 378, 2021, Art. no. 137935.

[19] A. M. Chockla, K. C. Klavetter, C. B. Mullins, and B. A. Korgel, "Solution-grown germanium nanowire anodes for lithium-ion batteries," *ACS Appl. Mater. Interfaces*, vol. 4, no. 9, pp. 4658–4664, 2012.

[20] E. Markevich, G. Salitra, and D. Aurbach, "Fluoroethylene carbonate as an important component for the formation of an effective solid electrolyte interphase on anodes and cathodes for advanced Li-ion batteries," *ACS Energy Lett.*, vol. 2, no. 6, pp. 1337–1345, 2017.

[21] R. Holze, "Huggins A. Robert: Advanced batteries–materials science aspects," *J. Solid State Electrochem.*, vol. 17, pp. 2371–2372, 2013. [Online]. Available: https://doi.org/10.1007/s10008-013-2093-4

[22] R. Huggins, *Advanced Batteries: Materials Science Aspects*. Berlin, Germany: Springer, 2008.

[23] Z.-C. Wang, J. Xu, W.-H. Yao, Y.-W. Yao, and Y. Yang, "Fluoroethylene carbonate as an electrolyte additive for improving the performance of mesocarbon microbead electrode," *ECS Trans.*, vol. 41, no. 41, 2012, Art. no. 29.

[24] D. McNulty, S. Biswas, S. Garvey, C. O'Dwyer, and J. D. Holmes, "Directly grown germanium nanowires from stainless steel: High-performing anodes for Li-ion batteries," *ACS Appl. Energy Mater.*, vol. 3, no. 12, pp. 11811–11819, 2020.

[25] S. Goriparti et al., "Facile synthesis of Ge–MWCNT nanocomposite electrodes for high capacity lithium ion batteries," *J. Mater. Chem. A*, vol. 5, no. 37, pp. 19721–19728, 2017.

[26] S. J. An et al., "The state of understanding of the lithium-ion-battery graphite solid electrolyte interphase (SEI) and its relationship to formation cycling," *Carbon*, vol. 105, pp. 52–76, 2016.

[27] X. Gao et al., "Fast ion transport in Li-rich alloy anode for high-energy-density all solid-state lithium metal batteries," *Adv. Funct. Mater.*, vol. 33, no. 7, 2023, Art. no. 2209715.

Valentina Diolaiti is currently a Ph.D. student with the Department of Physics and Earth Science, Univeristy of Ferrara, Ferrara, Italy.

Alfredo Andreoli is currently a Postdoc Researcher with the Department of Physics and Earth Science, Univeristy of Ferrara, Ferrara, Italy.

Susana Chauque is currently a Postdoc Researcher with Istituto Italiano di Tecnologia, Genova, Italy.

Paolo Bernardoni is currently a Researcher with the Department of Chemical, Pharmaceutical and Agricultural Sciences, University of Ferrara, Ferrara, Italy.

Giulio Mangherini is currently a Postdoc Researcher with the Department of Physics and Earth Science, Univeristy of Ferrara, Ferrara, Italy.

Marco Ricci is currently working toward the Ph.D. degree with the Istituto Italiano di Tecnologia, Genova, Italy and Department of Chemistry and Industrial Chemistry, University of Genova, Genova.

Remo P. Zaccaria is currently the Head of the DELTA Lab, Istituto Italiano di Tecnologia.

Matteo Ferroni is currently an Associated Professor with the Institute for Microelectronics and Microsystems CNR-Bologna Unit.

Donato Vincenzi is currently an Associated Professor, the Head of the Photovoltaic laboratory, University of Ferrara, Ferrara, Italy, and scientific Coordinator of ANGELS and GLITTERY projects.

Open Access funding provided by 'Università degli Studi di Ferrara' within the CRUI CARE Agreement